The Astrophysical Journal, 773:154 (10pp), 2013 August 20 doi:10.1088/0004-637X/773/2/154

CAUGHT IN THE ACT: THE ASSEMBLY OF MASSIVE CLUSTER GALAXIES AT $z = 1.62$

Jennifer M. Lotz[1], Casey Papovich[2], S. M. Faber[3], Henry C. Ferguson[1], Norman Grogin[1], Yicheng Guo[3], Dale Kocevski[4], Anton M. Koekemoer[1], Kyoung-Soo Lee[5], Daniel McIntosh[6], Ivelina Momcheva[7], Gregory Rudnick[8], Amelie Saintonge[9], Kim-Vy Tran[2,10], Arjen van der Wel[11], and Christopher Willmer[12]

[1] Space Telescope Science Institute, 3700 San Martin Drive, Baltimore, MD 21218, USA; lotz@stsci.edu
[2] George P. and Cynthia Woods Mitchell Institute for Fundamental Physics and Astronomy, and Department of Physics and Astronomy, Texas A&M University, College Station, TX, USA
[3] UCO/Lick Observatory, Department of Astronomy & Astrophysics, University of California, Santa Cruz, CA, USA
[4] Department of Physics & Astronomy, University of Kentucky, Lexington, KY, USA
[5] Department of Physics, Purdue University, West Lafayette, IN, USA
[6] Department of Physics & Astronomy, University of Missouri–Kansas City, 5110 Rockhill Road, Kansas City, MO, USA
[7] Department of Astronomy, Yale University, New Haven, CT, USA
[8] Department of Physics and Astronomy, University of Kansas, Lawrence, KS, USA
[9] Max-Planck-Institut für extraterrestrische Physik, D-85741 Garching, Germany
[10] Institute for Theoretical Physics, University of Zürich, CH-8057 Zürich, Switzerland
[11] Max-Planck-Institut für Astronomie, D-69117 Heidelberg, Germany
[12] Steward Observatory, University of Arizona, Tucson, AZ, USA

Received 2011 October 17; accepted 2013 June 7; published 2013 August 5

ABSTRACT

We present the recent merger history of massive galaxies in a spectroscopically confirmed proto-cluster at $z = 1.62$. Using *Hubble Space Telescope* WFC3 near-infrared imaging from the Cosmic Assembly Near-infrared Deep Extragalactic Legacy Survey, we select cluster and $z \sim 1.6$ field galaxies with $M_{\rm star} \geqslant 3 \times 10^{10}\,M_{\odot}$, to determine the frequency of double nuclei or close companions within projected separations less than 20 kpc co-moving. We find that four out of five spectroscopically confirmed massive proto-cluster galaxies have double nuclei, and $57\,^{+13}_{-14}\%$ of all $M_{\rm star} \geqslant 3 \times 10^{10}\,M_{\odot}$ cluster candidates are observed in either close pair systems or have double nuclei. In contrast, only $11\% \pm 3\%$ of the field galaxies are observed in close pair/double nuclei systems. After correcting for the contribution from random projections, the implied merger rate per massive galaxy in the proto-cluster is ∼3–10 times higher than the merger rate of massive field galaxies at $z \sim 1.6$. Close pairs in the cluster have minor merger stellar mass ratios ($M_{\rm primary}$:$M_{\rm satellite} \geqslant 4$), while the field pairs consist of both major and minor mergers. At least half of the cluster mergers are gas-poor, as indicated by their red colors and low 24 μm fluxes. Two of the double-nucleated cluster members have X-ray detected active galactic nuclei with $L_x > 10^{43}$ erg s^{-1}, and are strong candidates for dual or offset super-massive black holes. We conclude that the massive $z = 1.62$ proto-cluster galaxies are undergoing accelerated assembly via minor mergers, and discuss the implications for galaxy evolution in proto-cluster environments.

Key words: galaxies: clusters: general – galaxies: high-redshift – galaxies: interactions

Online-only material: color figures

1. INTRODUCTION

The assembly of the most massive galaxies in the universe has long been a classical problem for galaxy formation models. Today these objects have $\geqslant 10^{12}\,M_{\odot}$ of stars and live in the centers of galaxy clusters with $\geqslant 10^{14}\,M_{\odot}$ dark matter halos. Their stars are old with α-element enhancements that point toward an intense epoch of star-formation >10 Gyr ago (e.g., Thomas et al. 2005). However, their structures suggest a more chaotic formation. The most massive galaxies have elliptical morphologies, often with extended diffuse cD envelopes, boxy isophotes, and kinematics consistent with formation via multiple gas-poor spheroid–spheroid mergers (e.g., Boylan-Kolchin et al. 2005; Khochfar & Burkert 2003).

Current hierarchical galaxy formation models invoke late assembly times for very massive galaxies via mergers of smaller galaxies who have already formed the bulk of their stars (e.g., de Lucia & Blaziot 2007; Oser et al. 2012). Therefore a robust prediction of these models is that few exceptionally massive galaxies should exist in the early universe, and that their progenitors exist as many smaller sub-units at $z > 1$. In order to reconcile the difference between the star-formation histories and kinematic/morphological structures, the majority of stars are formed in the progenitors prior to merging. The subsequent assembly of these progenitors at $z < 1$ is expected to be largely dissipationless with little associated star-formation.

However, observations of the most massive galaxies at $z < 1$ are not entirely consistent with this picture. Some direct look-back studies at $z < 1$ have found little evolution in the most massive early-type galaxies. The number density of very bright (>2–4L^*) early-type galaxies has not evolved significantly since $z \sim 1$ (Cimatti et al. 2006; Scarlata et al. 2007; Mancone et al. 2010). The rest-frame luminosities and stellar masses of very bright distant galaxies suggest that ∼80% of the stars in today's most massive galaxies were already assembled by $z \sim 0.7$ or earlier (Brown et al. 2007; Stott et al. 2010). On the other hand, some studies find stronger evolution in the number density of galaxies with stellar masses $>10^{11}\,M_{\odot}$ (Ilbert et al. 2010; Brammer et al. 2011 but see Caputi et al. 2005). Strong evolution is also observed for lower mass typical L^* red galaxies, which double in number density and mass over the same epoch (e.g., Bell et al. 2004; Faber et al. 2007; Brown et al.

2007; Ilbert et al. 2010; Brammer et al. 2011). Direct evidence for mass growth by dissipationless merging is observed in some very luminous red galaxies and $z < 1$ clusters (e.g., Lauer 1988; Van Dokkum et al. 1999; Tran et al. 2005; White et al. 2007; Masjedi et al. 2008; McIntosh et al. 2008; Brough et al. 2011; Lidman et al. 2013), and give the inferred mass growth rates of 1%–20% per Gyr.

Although clusters and associated dark matter halos continue to grow by accreting groups, galaxy–galaxy mergers may be suppressed in virialized clusters because of the high relative velocities of cluster members (typically 500–1000 km s^{-1}). Matter recently accreted onto the central dark matter halo may be deposited into the satellite galaxy population and intracluster light, and not onto the central cluster galaxy (Brown et al. 2008; White et al. 2007; Conroy et al. 2007; Gonzalez et al. 2007; Rudnick et al. 2009). Galaxy groups with lower virial velocities (a few 100 km s^{-1}) are more conducive to galaxy mergers and the initial formation of massive red spheroidal galaxies than rich clusters (e.g., Tran et al. 2008). The $z < 1$ clusters which do show evidence of merging tend to be unrelaxed systems (e.g., MS1054: van Dokkum et al. 1999; Cl1604 : Kocevski et al. 2011). Likewise, high-redshift clusters and groups show a variety of star-formation densities relative to the field (e.g., Bauer et al. 2011; Hayashi et al. 2010; Fassbender et al. 2011; Snyder et al. 2012; Zeimann et al. 2012), suggesting a diversity of recent cluster assembly histories.

The best way to disentangle the merger and star formation histories of massive cluster galaxies is to study their progenitors in overdense regions at $z > 1.5$, i.e., in the environments expected to have the greatest galaxy merging and assembly and during the period when the bulk of their stars formed. If we want to catch these galaxies in the act of star-formation, these overdensities should not be biased toward galaxies which have already formed the bulk of their stars. Therefore the standard technique of selecting galaxy clusters via an overdensity of red galaxies may miss newly forming systems at high redshift. Likewise, if we want to catch these galaxies in the act of merging, these overdensities should not be biased toward virialized relaxed systems whose internal velocity dispersions will suppress mergers. Therefore Sunyaev–Zel'dovich and X-ray selected clusters may not be ideal places to study galaxy assembly, because their detection depends upon the presence of a halo of hot virialized gas and hence selects already relaxed systems.

In this paper, we study the recent merger history of massive galaxies in the spectroscopically confirmed overdensity XMM-LSS J02182-05102 at $z = 1.62$ (also known as IRC-0218A). This object was originally identified as a 20σ overdensity of high-redshift galaxies using an IRAC-color selection which identifies galaxies at $z > 1.3$ regardless of spectral type (Papovich 2008). Spectroscopic follow-up by Papovich et al. (2010) and Tanaka et al. (2010) confirmed 11 galaxies at $1.62 < z < 1.65$ within one projected physical Mpc of the central galaxy. A marginal detection of diffuse X-ray emission is associated with the overdensity (Papovich et al. 2010; Tanaka et al. 2010), and implies an upper limit on the virial mass $M_{200} \leqslant 7.7 \pm 3.8 \times 10^{13}\ M_{\odot}$ (Pierre et al. 2012). However the spatial structure of the overdensity indicates that it is not yet a virialized relaxed structure (Papovich et al. 2010). Likewise, the velocity dispersion is highly uncertain, with estimates ranging from 360 ± 90 km s^{-1} (Pierre et al. 2012) to 860 ± 490 km s^{-1} (Papovich et al. 2010). The spectroscopic and photometric-redshift members show evidence for a bright red sequence of galaxies (Papovich et al. 2010; Tanaka et al. 2010), as well as an excess of infrared luminous galaxies (Tran et al. 2010) and [O II] emitting galaxies (Tadaki et al. 2012). For the purposes of this paper, we will refer to XMM-LSS J02182-05102 as a "proto-cluster". In a hierarchical universe, this high-redshift overdensity is expected to grow by a factor of 5–10 in mass by present-day, consistent with the progenitor of a Virgo-like cluster (e.g., Papovich 2008; Springel et al. 2005).

We use high-spatial resolution *Hubble Space Telescope* Wide Field Camera 3 (*HST* WFC3) near-infrared F125W (*J*) and F160W (*H*) images from the Cosmic Assembly Near-infrared Deep Extragalactic Survey (CANDELS) pointing in the UKIDSS Deep Survey (UDS) field to trace the merger history, structure, and resolved colors of the massive proto-cluster members. The color–morphology and size–mass relations of the proto-cluster members are presented in a companion paper (Papovich et al. 2012). Throughout this work, we assume $\Omega_m = 0.3$, $\Omega_\Lambda = 0.7$, and $H_0 = 70$ km s^{-1} Mpc^{-1}.

2. OBSERVATIONS

CANDELS is an *HST* Multi-Cycle Treasury Program (PIs: S. M. Faber and H. C. Ferguson; see Grogin et al. 2011 and Koekemoer et al. 2011). CANDELS images five fields with the WFC3-IR camera (GOODS-N, GOODS-S, COSMOS, the Extended Groth Strip, and the UDS field) to two-orbit depth total in F125W (*J*) and F160W (*H*), with deeper pointings in the GOODS-N and GOODS-S fields. The reduced combined images were drizzled to a 0.″06 pixel scale. For the UDS CANDELS WFC3 imaging, the typical 5σ detection limits for a extended source is 27.1 ABmag in F125W and 26.9 ABmag in F160W. The parallel Advanced Camera for Surveys (ACS) imaging of the UDS field reaches typical 5σ extended source detection limits of 27.2 ABmag in F606W and F814W. The UDS field (UDS) was the first CANDELS field to be completed in 2011 January.

The UDS galaxies were detected and measured in the *HST* F160W WFC3 images using SExtractor v2.5.0 (Bertin & Arnouts 1996) in combined "hot" and "cold" detection runs (Galametz et al. 2013). The majority of the objects presented here were detected in the "cold" run with the detection threshold set to 0.75σ, detection MINAREA = 5 pixels, and a 9×9 pixel tophat convolution kernel. The combined F160W "hot + cold" segmentation map was then used as an input template to perform multi-wavelength photometry on ground-based (Subaru *BVRIz*, UKIRT *K*), *Spitzer* (IRAC channels 1–4), and other *HST* (ACS F606W, F814W; WFC3 F125W) images from the Subaru-*XMM* Deep Survey (Furusawa et al. 2008), UKIRT IR Deep Sky Survey[13] (O. Almani et al., in preparation; Williams et al. 2009), *Spitzer* Extended Deep Survey[14] (PI: F. Giovanni), *Spitzer* UDS program[15] (PI: J. Dunlop) and CANDELS respectively, using the TFIT software (Laidler et al. 2007).

Photometric redshifts and stellar masses were calculated for the entire CANDELS–UDS field based upon the combined multi-wavelength photometry catalog. Photometric redshifts and probability distributions were computed using EAZY code (Brammer et al. 2008). We have compared the photometric redshifts to UDS spectroscopic redshift catalogs (M. Akiyama et al., in preparation; M. C. Cooper et al., in preparation; Simpson et al. 2012; Smail et al. 2008) and find mean

[13] http://www.nottingham.ac.uk/astronomy/UDS/data/dr3.html
[14] http://www.cfa.harvard.edu/SEDS
[15] http://irsa.ipac.caltech.edu/data/SPITXER/SpUDS

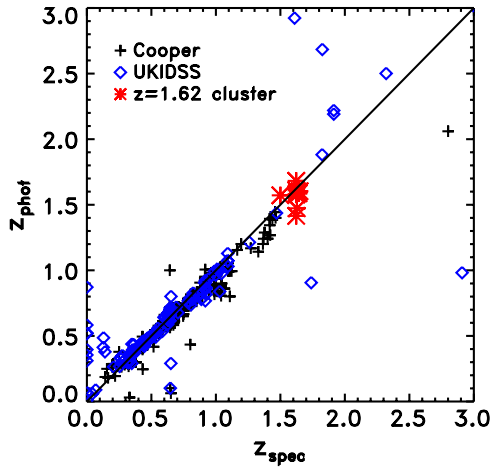

Figure 1. Spectroscopic redshift vs. photometric redshift for UDS galaxies based on the CANDELS *HST* + ground-based UKIDSS + *Spitzer* SEDS TFIT-derived photometric catalog. The UDS field spectroscopic redshifts are from Cooper et al. (black crosses) and the public UDS compilation (Akiyama et al., in preparation; Simpson et al. 2012; Smail et al. 2008). We also plot the six spectroscopic redshifts for cluster members within the CANDELS–UDS field from Tanaka et al. (2010) and Papovich et al. (2010) (red asterisks). We find $\langle \delta z/(1+z_{\rm spec})\rangle = 0.05$), with 5% catastrophic outliers with $\delta z/(1+z_{\rm spec}) \geqslant 0.3$.

(A color version of this figure is available in the online journal.)

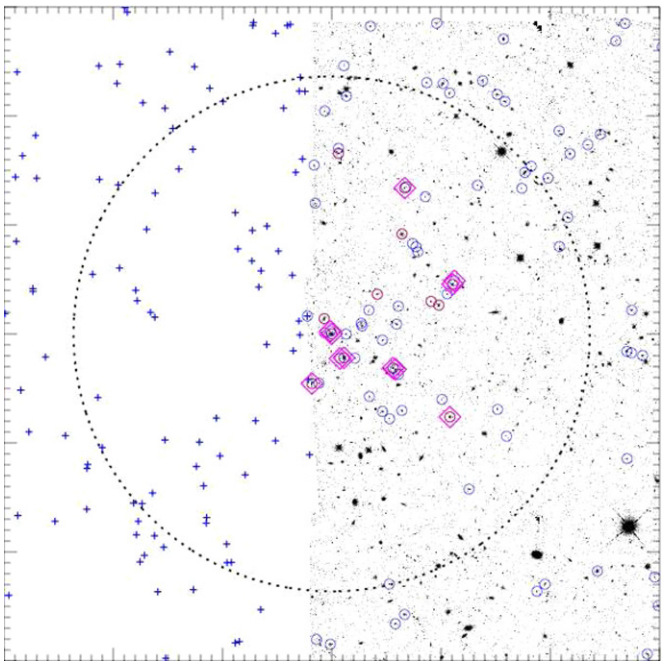

Figure 2. Proto-cluster candidate members are over-plotted on a $200'' \times 200''$ FOV centered on the central cluster galaxy 19085. The CANDELS–UDS *HST* WFC3 F160W image covers only the right half of this FOV. Objects with $\mathcal{P}_{\rm zcl} > 0.3$ from the CANDELS–UDS photometric redshift catalog are plotted as blue circles; objects with $\mathcal{P}_{\rm zcl} > 0.3$ from ground-based photometric redshift catalog are plotted as blue crosses. Cluster candidates with stellar masses $>3 \times 10^{10}\,M_{\odot}$ are plotted as red circles, and mergers are magenta diamonds. The merger and the massive cluster candidates all lie well within one projected Mpc (dotted circle; co-moving).

(A color version of this figure is available in the online journal.)

$\langle \delta z \rangle = 0.05(1+z)$, with ∼5% catastrophic outliers with $\delta z > 0.3(1+z)$ (Figure 1). The six spectroscopically confirmed cluster members which lie within the CANDELS footprint have similarly good agreement between their spectroscopic and photometric redshifts ($\delta z/(1+z_{\rm spec}) \sim 0.05$). We have examined the effect of excluding the lower-spatial resolution IRAC photometry on the photometric redshifts, and find a negligible difference in the overall photometric redshifts and the selected cluster candidates. This is because the *HST* segmentation maps are used as a prior for the multi-band photometry, and the photometric redshifts at $z \sim 1$–2 are strongly influenced by the 4000 Å break in the *I*, *z*, and F125W observed bands.

Stellar masses were computed assuming Bruzual & Charlot (2003) stellar population models, solar metallicities, a Chabrier (2003) initial mass function (IMF), and Calzetti et al. (2000) extinctions (see Papovich et al. 2001, 2006 for details). Based upon the 68% confidence intervals of the redshift probability distributions, the median uncertainty in the stellar masses is ∼20%–30% at $z \sim 1.6$ and $M_{\rm star} > 3 \times 10^{10}\,M_{\odot}$. (This value does not include the uncertainties resulting from uncertainties in the spectral energy distribution (SED) fitting from extinction, star-formation history, and the stellar IMF.) At $z \sim 1.6$, the stellar mass limit is roughly $\sim 1 \times 10^{10}\,M_{\odot}$ for quiescent galaxies and $\sim 3 \times 10^{9}\,M_{\odot}$ for star-forming galaxies (Bassett et al. 2013).

We follow Papovich et al. (2010, 2012) and Bassett et al. (2013) and select proto-cluster candidates using the integrated redshift probability

$$\mathcal{P}_{\rm zcl} \equiv \int_{0.05(1-z_{\rm cl})}^{0.05(1+z_{\rm cl})} P(z)dz \qquad (1)$$

where $z_{\rm cl} = 1.625$. Red proto-cluster candidates typically have $\mathcal{P}_{\rm zcl} > 0.5$. Spectroscopically confirmed proto-cluster members with star-forming SEDs have less constrained photometric redshift probability distributions and integrated $\mathcal{P}_{\rm zcl} \sim 0.3$. Therefore we require $\mathcal{P}_{\rm zcl} > 0.3$ for proto-cluster candidacy in order to include both quiescent and star-forming galaxies. We will discuss field galaxy contamination in our photometric redshift proto-cluster candidates in the following section.

We have also matched the UDS samples to the *Spitzer* MIPS 24 μm photometric catalog (Tran et al. 2010) obtained by SpUDS[15]. The 24 μm fluxes and spectroscopic or photometric redshifts were used to compute star-formation rates. At $z = 1.62$, the observed 24 μm flux arises from rest-frame ∼8–10 μm emission, which can include strong polycyclic aromatic hydrocarbon emission features and silicate absorption (e.g., Smith et al. 2007; Snyder et al. 2013). We adopt the Rujopakarn et al. (2013) redshift-dependent conversions to extrapolate to a total infrared luminosity and corresponding star-formation rate. Note that the Rujopakarn et al. (2013) conversion gives at factor of ∼2 lower star-formation rates for our sources than the Chary & Elbaz (2001) templates. The 3σ detection limit of the MIPS 24 μm catalog is ∼40 μJy or $\sim 20\,M_{\odot}$ yr^{-1} at $z \sim 1.62$.

The XMM-LSS J02182-05102 proto-cluster is serendipitously located in the edge of the CANDELS WFC3-IR imaging of the UDS field. The proto-cluster is only partially covered by WFC3 and has no ACS parallel coverage (Grogin et al. 2011; Figure 2). Nevertheless, 6 out of 11 spectroscopically confirmed proto-cluster galaxies (including the central proto-cluster galaxy) are located within the CANDELS UDS observations. Five of these objects have best-fit stellar masses greater than $3 \times 10^{10}\,M_{\odot}$ and are included in our massive proto-cluster galaxy sample (Table 1; Figure 3). We select 9 additional proto-cluster member candidates with $\mathcal{P}_{\rm zcl} > 0.3$, projected separation <1 Mpc from the central proto-cluster galaxy, and stellar masses $>3 \times 10^{10}\,M_{\odot}$ (Figure 4). Finally, based on the

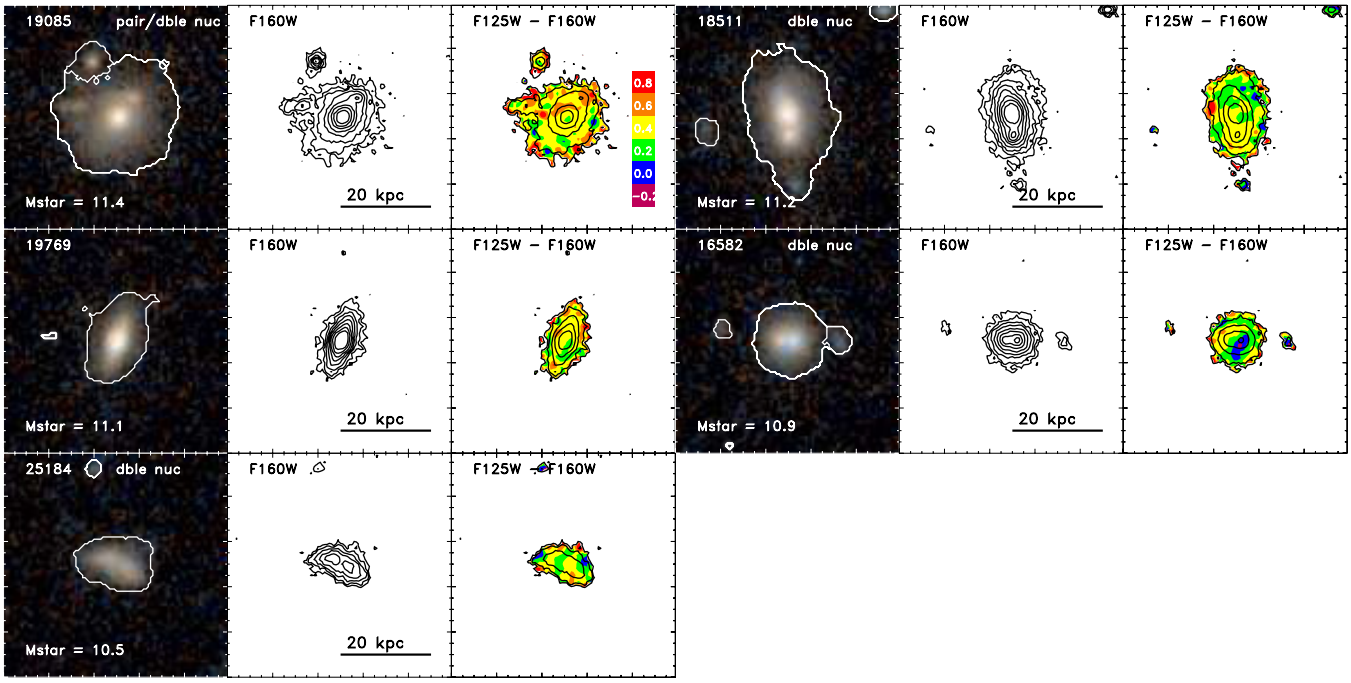

Figure 3. Spectroscopically confirmed $M_{\rm star} > 3 \times 10^{10}\,M_{\odot}$ cluster members. Left panels: RGB color maps from F160W/F125W+F160W/F125W images. The F160W segmentation maps are shown as white contours. Center: F160W surface-brightness contours, at $\mu_{\rm H} = 20.5$–24 in 0.5 mag arcsec^{-2} intervals. Right: F125W − F160W color maps where $\mu_{\rm H} < 24.0$. Four of the five massive cluster members have double nuclei/satellites separated by less than 20 co-moving kpc. The images are $6'' \times 6''$.

(A color version of this figure is available in the online journal.)

Table 1
Interacting/Merging Galaxy Counts

Sample	$N_{\rm total}$	$N_{\rm merg}$[a]	$N_{\rm dblenuc}$[b]	$N_{\rm comp}$[c]	$f_{\rm merg}$(obs)	$C_{\rm proj}$[d]	$C_{\rm field}$[e]	$f_{\rm merg}$(cor)
Cluster $z_{\rm spec}$ only	5	4	4	1	80^{+13}_{-23}%	22% ± 11%	N/A	58^{+17}_{-25}%
Cluster all	14	8	5	3	57^{+13}_{-14}%	22% ± 11%	0.45/5	49% ± 18%
Field $z \sim 1.6$	130	14	3	11	11% ± 3%	1.4% ± 1.0%	N/A	9% ± 3%

Notes.

[a] The number of unique $M_{\rm star} \geqslant 3 \times 10^{10}\,M_{\odot}$ galaxies in a merger, defined as having a double nucleus and/or close companion.

[b] The number of merging galaxies with double or multiple bright nuclei within the SExtractor-defined segmentation map (see Figures 3 and 4).

[c] The number of merging galaxies with one or more distinct close companions within 20 kpc co-moving and $\mathcal{P}_{\rm zcl} > 0.3$. Pairs where both objects have $M_{\rm star} \geqslant 3 \times 10^{10}\,M_{\odot}$ are counted twice.

[d] The probability of chance projections at $\leqslant 2''.4$ for each sample, based on Monte Carlo simulations. See Section 3 for details.

[e] The number of projected $z \sim 1.6$ $M_{\rm star} \geqslant 3 \times 10^{10}\,M_{\odot}$ field mergers and total galaxies contaminating the cluster photometric-redshift selected sample, based on the surface density of field galaxies and field merger fraction.

same dataset, we select a control sample of 130 field galaxies with $\mathcal{P}_{\rm zcl} > 0.3$, projected separation >2 Mpc from the central proto-cluster galaxy, and best-fit stellar masses $\geqslant 3 \times 10^{10}\,M_{\odot}$. Based upon the surface density of the control sample, we expect that ∼5 photometric-redshift proto-cluster candidates may be background/foreground field galaxies.

3. MERGER RATE IN PROTO-CLUSTER VERSUS FIELD

We identified merger candidates within our proto-cluster and control samples as objects with double nuclei within the galaxy and/or close companions at a projected separation less than 20 kpc co-moving. While the vast majority of galaxies are cleanly detected and de-blended in our *HST* F160W segmentation map, the distinction between galaxies with double nuclei and close pairs are particularly challenging for galaxy detection algorithms. In order to avoid incompleteness in our merger candidate samples, we visually inspected the F160W contour maps of all proto-cluster and control sample galaxies for double nuclei within the SExtractor-defined segmentation maps (Figures 3–5) as well as searched for *HST*-detected companions within ∼20 co-moving projected kpc ($2''.4$) and $\mathcal{P}_{\rm zcl} > 0.3$. We do not place stellar mass constraints on the companions, but note that the lowest mass companions have $M_{\rm star} \sim 8 \times 10^{9}\,M_{\odot}$. Because we use the same dataset for the control and cluster samples, we expect both samples to have the same biases in their photometric redshifts, stellar masses, colors, and merger selections.

The interacting galaxy statistics for the cluster and control field sample are summarized in Table 1. We found that four out of the five spectroscopic proto-cluster members have evidence of

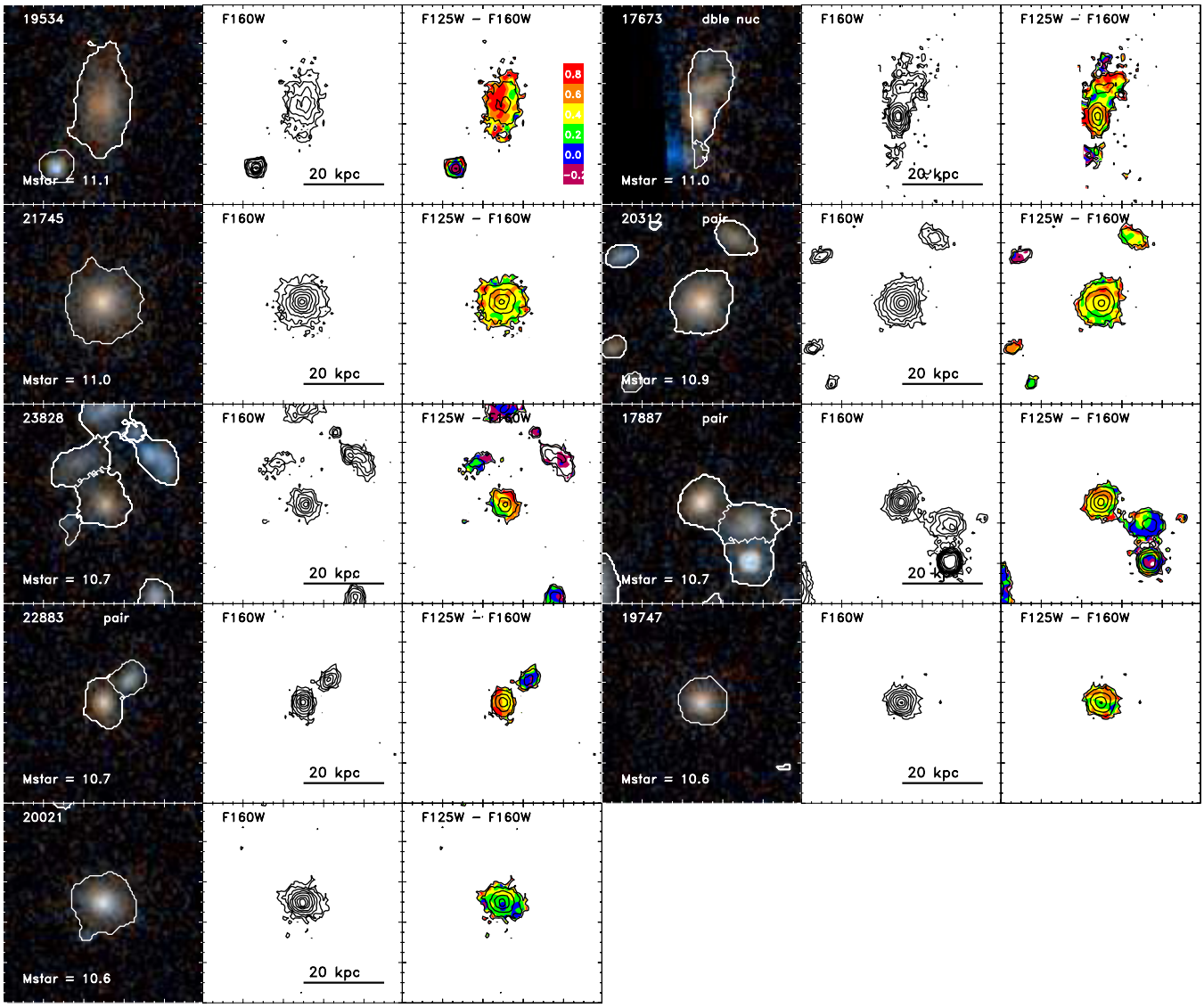

Figure 4. Additional photometric-redshift selected proto-cluster candidates ($M_{\rm star} \geqslant 3 \times 10^{10}\,M_{\odot}$, $P(z) > 0.3$, and projected distance from central cluster galaxy <1 Mpc). Four photometric-redshift proto-cluster candidates meet the merger criteria of a double nucleus or close companion brighter with $\mathcal{P}_{\rm zcl} > 0.3$ within 20 co-moving kpc. The image sizes, contours, and scalings are the same as Figure 3.

(A color version of this figure is available in the online journal.)

Table 2
Spectroscopically Confirmed Massive Cluster Galaxy Properties

CANDELS ID	$z_{\rm spec}$	α (J2000)	δ (J2000)	$H_{\rm AB}$	log10[$M_{\rm star}$] ($M_{\odot}$)	f_{24}[a] (μJy)	SFR[b] ($M_{\odot}$ yr^{-1})	L_x[0.5–2 keV][c] (10^{43} erg s^{-1})
19085[d]	1.634[e]	34.58977	−5.17219	20.78	11.4	...	...	...
18511	1.623[e]	34.58788	−5.17583	20.55	11.2	...	...	1.6 ± 0.3
19769	1.642[e]	34.57336	−5.16781	21.05	11.1	...	...	...
16582	1.649[e,f]	34.57166	−5.18490	21.57	10.9	79 ± 3	50	2.7 ± 0.4
25184	1.622[f]	34.56322	−5.13663	22.22	10.5	121 ± 4	86	...

Notes.
[a] 24 μm fluxes from Tran et al. (2010), SpUDS observations (http://irsa.ipac.caltech.edu/data/SPITXER/SpUDS); 1σ detection limit $\sim$30 μJy.
[b] Star-formation rates are calculated from observed f_{24} and spectroscopic redshifts, assuming the redshift-dependent Rujopakarn et al. (2013) conversion of f_{24} to L(TIR).
[c] Based on *Chandra* soft X-ray fluxes from Pierre et al. (2012). Rest-frame 0.5–2 keV luminosities are calculated assuming the spectroscopic redshift and a power-law spectrum with index = 1.4.
[d] Assumed central cluster galaxy.
[e] Tanaka et al. (2010).
[f] Papovich et al. (2010).

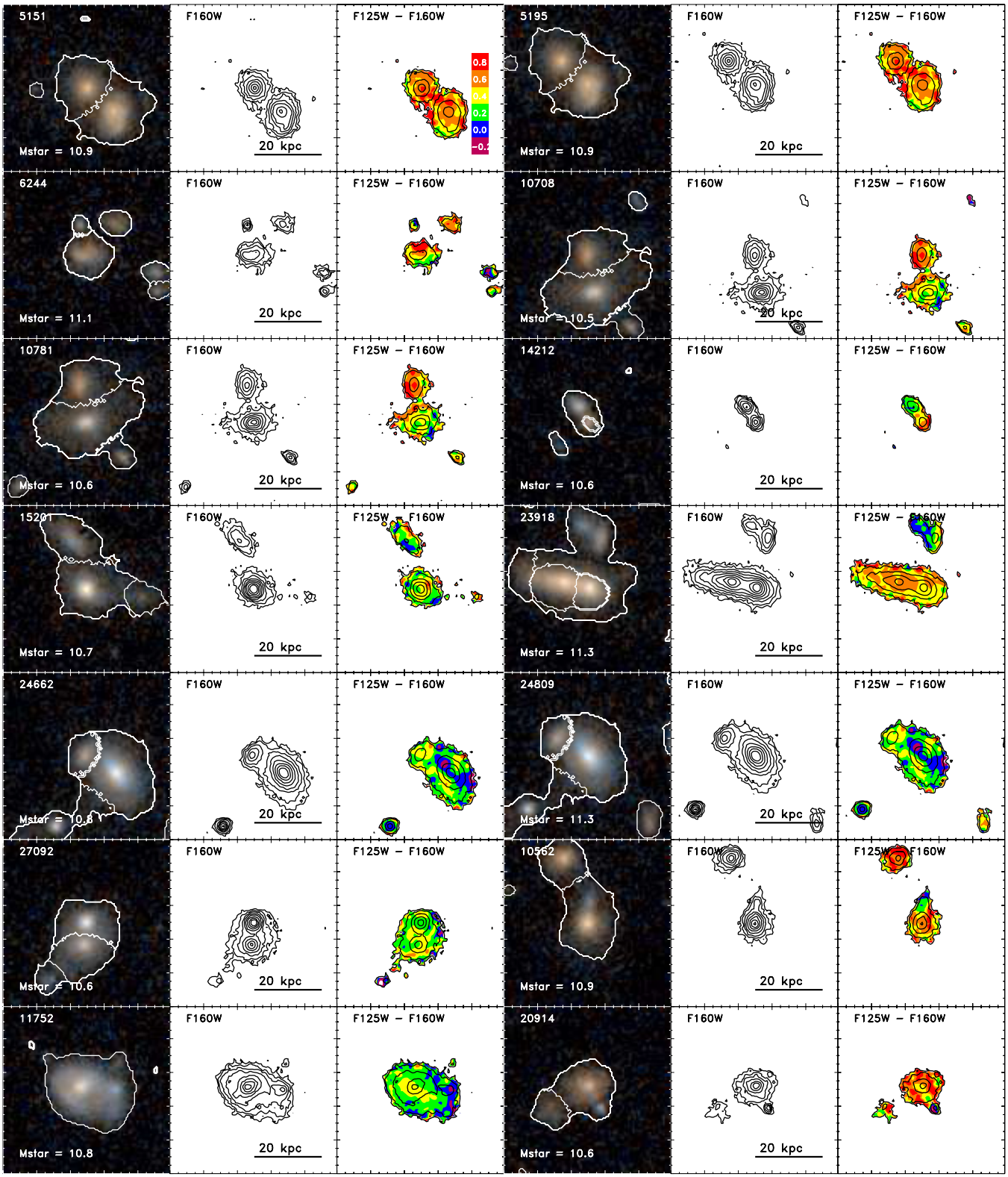

Figure 5. Double nuclei/close pair candidates from the UDS control sample ($M_{\rm star} > 3 \times 10^{10}\,M_{\odot}$, $\mathcal{P}_{\rm zcl} > 0.3$, and projected distance from central proto-cluster galaxy >2Mpc). Fourteen UDS control objects show double nuclei or a close companion with $\mathcal{P}_{\rm zcl} > 0.3$ separated by less than 20 co-moving kpc, resulting in 11 unique systems. The white contours show the F160W segmentation map.

(A color version of this figure is available in the online journal.)

double/multiple nuclei in their F160W contour maps, including 19085 which has both a close companion and multiple nuclei (Table 2, Figure 3). Out of the nine additional photometric proto-cluster candidates, 1 has multiple components, and three objects have companions within 20 kpc with $\mathcal{P}_{\rm zcl} > 0.3$. Of the control sample, we find 14 unique galaxies with a double nucleus and/or close companion, including 3 pairs of galaxies where both companions are more massive than $3 \times 10^{10}\,M_{\odot}$, and

one object with both a second nucleus and a close companion. The total number of merging $M_{\rm star} \geqslant 3 \times 10^{10}\,M_{\odot}$ progenitor galaxies is given as $N_{\rm merg}$, and the observed (uncorrected) merger fractions are listed as $f_{\rm merg}$ in Table 1. For the cluster, the observed merger fractions are 80^{+13}_{-23}% for the spectroscopic sample and 57^{+13}_{-14}% for the full cluster sample. The observed merger fraction in the field is 10.7% ± 3%. Uncertainties were computed assuming a binomial distribution with the *R* statistical package[16] routine binom.confint).

However, these merger fractions are likely an overestimate of the true merger fraction because of both contamination of by both objects at the same photometric redshift but not physically associated with another, and by objects close in real space that do not actually merge. We estimate the false pair contamination $C_{\rm proj}$ (Table 1) as the probability of another $\mathcal{P}_{\rm zcl} > 0.3$ UDS galaxy randomly falling within 20 kpc projected of our primary galaxy sample. For the field sample, we randomized the R.A. and decl. positions of all $\mathcal{P}_{\rm zcl} > 0.3$ $M_{\rm star} > 3 \times 10^{9}\,M_{\odot}$ field galaxies the 1000 times and determine the fraction of $M_{\rm star} > 3 \times 10^{10}\,M_{\odot}$ galaxies with a randomly projected companion. The position randomization treats each individual galaxy in the original close pair systems separately while the components of the doubly nucleated galaxies are treated as a single object. The average fraction of false companions per primary galaxy is 1.4% ± 1.0%. Correcting for this contamination gives a field merger fraction 9% ± 3%. Recent studies of field samples at $z \sim 2$ find pair fractions ∼5%–18% for projected separations <30 physical kpc h^{-1} and stellar mass ratios between 1:1 and 10:1 (Williams et al. 2011; Man et al. 2012; Newman et al. 2012). Our field pair fraction at $z \sim 1.6$ is consistent with these measurements, assuming the timescale for identifying close pairs at projected <30 physical kpc is roughly twice the timescale for finding pairs at <20 co-moving (7 physical) kpc (e.g., Lotz et al. 2010).

We also estimate the false pair contamination rate $C_{\rm proj}$ for the proto-cluster galaxy sample. The proto-cluster is an overdense region and false pairs may arise from galaxies associated with the proto-cluster but are not interacting. In order to maintain the proto-cluster's density profile, we randomly scattered the positions of all 67 proto-cluster candidates ($\mathcal{P}_{\rm zcl} > 0.3$, < 1 Mpc from central proto-cluster galaxy, $M_{\rm star} > 3 \times 10^{9}\,M_{\odot}$) to within 10″ of their original positions 1000 times. We find that the average fraction of false companions per massive proto-cluster galaxy is 22% ± 11%; this contamination rate declines if we increase the scattering radius or allow the galaxies to be randomly place within the window 1 Mpc from the central cluster galaxy and within the CANDELS observations (Figure 1). For the spectroscopic cluster sample, we derive a corrected merger fraction of 58^{+17}_{-25}%. If we further assume that five photometric-redshift selected cluster candidates are interloping field galaxies, including 0.45 field mergers ($C_{\rm field}$ in Table 1), we derive a corrected merger fraction for the entire cluster sample of 49% ± 18%.

In summary, we derive corrected merger fractions 58^{+13}_{-23}% for the spectroscopic cluster sample, 49% ±18% for the combined spectroscopic and photometric redshift proto-cluster samples, and 9% ± 3% for the field control sample. We have not estimated a correction factor for those objects which are close in real space but do not actually merge. This factor is typically estimated to be ∼0.5 (Patton & Atfield 2008), but is likely to also depend upon the clustering strength (e.g., Bundy et al. 2009). Assuming that the dynamical friction timescales, mass ratios, and non-merging pair corrections for the proto-cluster and control samples are similar, then the implied proto-cluster merger rate is ∼3–10 times greater than the field merger rate at $z \sim 1.6$. We argue that the sub-components and companions associated with each proto-cluster galaxy are within close physical proximity and have a high probability of merging within 1–2 Gyr (by redshift ∼1). Our simulations imply that the majority of close pairs in the cluster are not non-interacting proto-cluster galaxies viewed in projection. The spatial distribution of galaxies and X-ray structure of the over-density suggest that it consists of several groups which have not yet formed a virialized proto-cluster. Therefore the relative velocities of galaxies in close proximity are likely low enough for a mergers (i.e., a few hundred km s^{-1} found in group environments) rather than a large relative velocities (500–1000 km s^{-1}) found in massive proto-cluster environments.

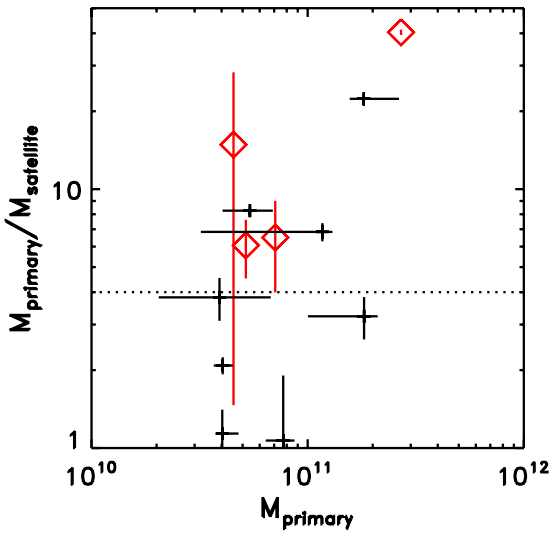

Figure 6. Stellar mass ratio for the four proto-cluster pairs (red diamonds) and eight field pairs (black crosses) as a function of primary galaxy stellar mass. Major mergers have $M_{\rm primary}/M_{\rm satellite} < 4$ (dashed line), while this ratio for minor mergers is >4. The error-bars on the stellar mass ratios are based on the 68% confidence intervals for the photometric redshift uncertainty, and do not include additional uncertainties due to extinction and star-formation history.

(A color version of this figure is available in the online journal.)

We examine the stellar mass ratios of the close pairs as a function of the primary galaxy stellar mass in Figure 6. The four pairs in the proto-cluster have "minor" merger stellar mass ratio $M_{\rm primary}/M_{\rm satellite} > 4{:}1$. In contrast, the field pairs are more likely to have "major merger" stellar mass ratios ∼1:1–4:1. Our sample is too small to draw strong conclusions, but suggest that minor mergers are playing a dominant role in the buildup of the massive proto-cluster galaxies. Determining the stellar mass ratios of the multiple nuclei systems is hampered by the lack of high-resolution *HST* data blueward of the 4000 Å break, and is beyond the scope of this paper. The proto-cluster mergers may have longer dynamical friction timescales than the typical field pairs if they have systematically greater mass ratios and/or higher relative velocities. Simple dynamical friction arguments (Binney & Tremaine 1987) imply that the decay time scales as $M_{\rm primary}/M_{\rm satellite}$. In the extreme case that all detected proto-cluster mergers are minor mergers with typical merger timescales ∼ three times the field sample, then number of mergers per massive proto-cluster galaxy is roughly 2–3 times greater than the field merger rate.

[16] http://www.R-project.org

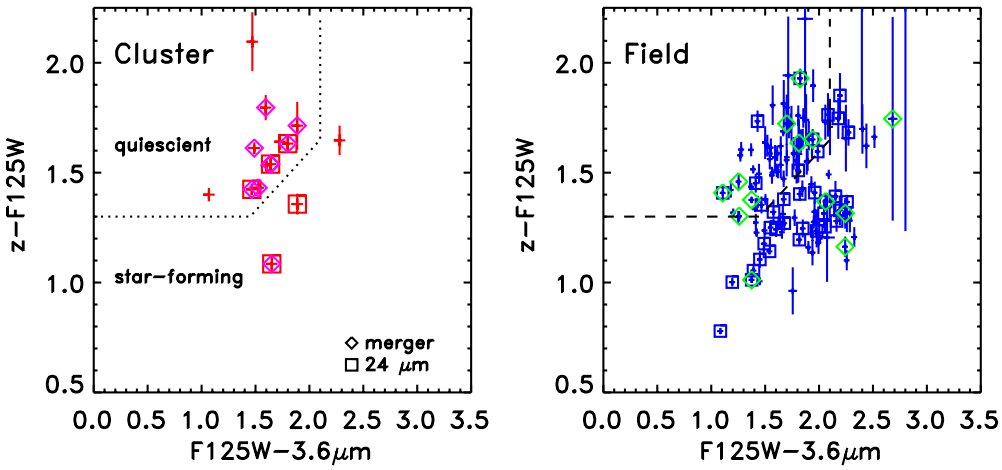

Figure 7. Observed *HST* F125W − IRAC 3.6 μm vs. Subaru z − F125W colors for the proto-cluster members (left) and control field samples (right) with $M_{star} \geqslant 3 \times 10^{10} M_{\odot}$. Merger candidates are marked with diamonds. MIPS 24 μm detections are marked with squares. Most of the proto-cluster mergers have quiescent colors, while only one cluster merger has colors consistent with on-going star-formation.

(A color version of this figure is available in the online journal.)

4. RECENT STAR-FORMATION HISTORIES OF MERGERS

We examine the $J-H$ color maps (Figures 3–5) to constrain the relative colors of the merging pairs, and find that the mergers consistent of red–red or mixed red-blue pairs. Observed $J-H$ is roughly rest-frame $B-R$ (0.48–0.61 μm) at $z = 1.625$. We find that the two most massive proto-cluster galaxies are consistent with red-red galaxy mergers. 19085 is a massive red spheroidal galaxy (see Papovich et al. 2012) with two or three additional nuclei/companions of similar $J-H$ color ($\sim$0.4). 18511 is a spheroid-dominated galaxy of $\sim$0.2 mag bluer in $J-H$ color than 19085 with a redder second nucleus. The less massive proto-cluster merger 16582 has one red nucleus ($J-H = 0.4$) and one blue nucleus ($J-H = -0.2$). 25184 has a double-peaked H-band surface brightness profile, $J-H \sim 0.2$–0.4 colors, and a disky structure consistent with either a double nucleus or patchy dust. None of the photometric redshift proto-cluster merger candidates have observed $J-H$ colors bluer than 0.2 for both components. In contrast, many of the field mergers are blue with one or both components showing $J-H < 0.2$.

Following Papovich et al. (2012), we also use the integrated $z-F125W$ and $F125W-3.6\,\mu$m colors to constrain whether the massive cluster and field galaxies are "quiescent" or "star-forming" (Figure 7). At $z \sim 1.6$, these observed colors are similar to the rest-frame $U-V$ and $V-J$ colors used by Wuyts et al. (2007) and Williams et al. (2009) to distinguish between galaxies with relatively low star-formation rates and UV-bright/dusty galaxies with high star-formation rates. We find that proto-cluster galaxies are more likely to be quiescent in the $z-$F125W versus F125W − 3.6 μm plot than the field sample (79% versus 50%), with the merger samples following the color distributions of their parent samples (75% of cluster mergers are quiescent, versus 57% of the field mergers), consistent with Bassett et al.'s (2013) findings for the proto-cluster core and surrounding field. To determine the significance of the different color distributions for the cluster and field galaxies, we have bootstrapped the color distribution of the field sample of 130 galaxies, randomly selected N bootstrapped objects (where $N =$ 14 for the 14 massive cluster candidates), and calculated the fraction of quiescent galaxies 10,000 times. The bootstrapped photometric errors are assumed to follow a normal distribution with $\sigma \sim 3\times$ the TFIT-derived photometric errors (typically a few percent). We find that the high quiescent fraction for the cluster galaxies($\geqslant$11/14) is reproduced by the bootstrapped field-galaxy selection less that 1.4% of the time, and the high quiescent for the cluster mergers ($\geqslant$6/8) is reproduced less than 9% of the time. We conclude that the cluster sample has significantly more quiescent objects than the field population, and that the cluster merger star-formation histories reflect those of the parent cluster sample. On the other hand, the quiescent fraction of field mergers (8/14) is completely consistent with being randomly drawn from the general field population.

We have matched the proto-cluster candidates to the *Spitzer* MIPS 24 μm sources within 3″. Five proto-cluster candidates have 3σ detections, including four mergers and three objects which are classified as quiescent in Figure 7. For comparison, 39 objects in the control sample are detected as 24 μm sources, including six merging systems. Assuming the 24 μm flux arises from star-formation rather than active galactic nucleus (AGN) activity, the proto-cluster mergers have star-formation rates $\sim$50–150 $M_{\odot}$ yr^{-1}. However, one of the proto-cluster 24 μm sources (16582) is also a *Chandra* X-ray detection with an AGN-like X-ray luminosity. We conclude that at least half of the proto-cluster mergers are dissipationless as indicated by their colors and low 24 μm fluxes; this fraction is likely to be higher if low-luminosity AGNs are a significant source of observed 24 μm emission (e.g., Snyder et al. 2013).

5. AGNs IN PROTO-CLUSTER MERGERS

Two of the spectroscopically confirmed proto-cluster member are point sources in recent *Chandra* imaging of the proto-cluster (Pierre et al. 2012). For these two massive proto-cluster galaxies, the growth of their central super-massive black holes (SMBH) via accretion and black-hole mergers is coincident with the assembly of their stellar components. CANDELS UDS object 18511 has a [0.5–2 keV] X-ray flux $= 1.60^{+0.36}_{-0.34} \times 10^{-15}$ erg cm^{-2} s^{-1} (Pierre et al. 2012), which implies an X-ray luminosity at $z = 1.623$ of L_x [0.5–2 keV] $= 1.6 \times 10^{43}$ erg s^{-1}, consistent with AGN activity. This object has a bright central nucleus and a close secondary nucleus less than 5 kpc away. CANDELS UDS object 16582 also has an X-ray AGN with [0.5–2 keV] X-ray flux $= 2.69^{+0.44}_{-0.42} \times 10^{-15}$ erg cm^{-2} s^{-1},

corresponding to L_x [0.5–2 keV] $= 2.7 \times 10^{43}$ erg s^{-1}. This object has a double nucleus with no clear dominant central component. Assuming the AGN activity is associated with one or both stellar nuclei, then this object is a strong candidate for an offset or dual AGNs. Confirmed dual AGNs separated by a few kiloparsecs have been observed only in a handful systems, largely at $z \sim 0$ (e.g., Comerford et al. 2011; Komossa et al. 2003), notably in the center of the nearby rich proto-cluster A400 (Hudson et al. 2006). An offset AGN is also an intriguing possibility, as either a signature of a SMBH–SMBH merger in which only one SMBH is visible or a possible gravitational wave recoiling black hole (e.g., Civano et al. 2010). A third X-ray AGN is detected in the proto-cluster (Pierre et al. 2012), but this object is not within the CANDELS WFC3 data. Finally, we note that the current *Chandra* observations are fairly shallow (84 ks), and that rest-frame optical emission line diagnostics suggest that low-luminosity AGNs are fairly common in this proto-cluster (M. Peth et al., in preparation).

6. IMPLICATIONS FOR MASSIVE GALAXY ASSEMBLY

The implied merger rate for the massive proto-cluster galaxies is extremely high. For galaxies with double nuclei and/or projected separations less than ∼7 kpc physical (∼20 kpc co-moving at $z = 1.62$) and stellar mass ratios ∼1:1–1:10, the merger detection timescale is ∼0.20 Gyr (Lotz et al. 2010, 2011). Adopting a proto-cluster pair fraction between 40%–80% and assuming all of the observed pairs will merge, this gives a merger rate of ∼2–4 mergers per Gyr per galaxy for the proto-cluster galaxies, as compared to ∼0.5 mergers per Gyr per galaxy in the field.

Such a high merger rate points to accelerated assembly of the proto-cluster galaxies relative to the field. Papovich et al. (2012) finds that the sizes of quiescent proto-cluster galaxies are significantly larger than the $z \sim 1.6$ field population at a fixed stellar mass, implying that the proto-cluster early-types have undergone more rapid size growth their recent past. Evidence for accelerated evolution in over-dense environments as early as $z \sim 2$ has been found by several other recent studies (Nipoti et al. 2012; Zirm et al. 2012; Cooper et al. 2012). Comparison of the red-sequence luminosity function of this proto-cluster to those in clusters at $z < 0.8$ suggests that red galaxy merging over this epoch significantly alters the cluster galaxy luminosity function (Rudnick et al. 2012). The presence of X-ray AGN in two double-nucleated systems suggests that the SMBH of some $z = 1.62$ proto-cluster galaxies are growing via accretion and black-hole mergers at the same time as the assembly of their stars.

The assembly history of XMM-LSS J02182-05102 proto-cluster galaxies are largely consistent with the predictions of de Lucia & Blaziot (2007) for the progenitors of massive proto-clusters galaxies at this epoch. The de Lucia & Blaziot model predicts that the eventual brightest proto-cluster galaxies have only assembled 20% of their stars by $z \sim 1.5$. The most massive proto-cluster galaxies in our sample are $1–2 \times 10^{11}\ M_\odot$, consistent with this 20% value. However, it is not entirely clear if massive proto-cluster galaxies can grow quickly enough to be consistent with being largely assembled by $z \sim 0.8$. In order for the most massive proto-cluster galaxy at $z = 1.62$ to grow into a $\sim 8 \times 10^{11}\ M_\odot$ galaxy by $z \sim 0.8$, it would need to quadruple its mass. This requires at least 1 major merger and ∼8–10 minor mergers in a 2.7 Gyr time period (assuming >6:1 mass ratio and $M_{\rm sat} \sim 3 \times 10^{10}\ M_\odot$). This is on the high end of our observed merger rate of 2–4 mergers per Gyr, and assumes that the merging timescales do not evolve significantly either with the growth of the brightest cluster galaxy or with the virialization of the proto-cluster.

The same models also predict that >90% of the brightest cluster galaxy stars are formed by $z \sim 2$, well before their assembly into a single massive galaxy. The majority of massive proto-cluster mergers are "quiescent" relative to the full galaxy population at $z \sim 1.6$, suggesting that they have already begun to quench their star-formation. Their SEDs and SFRs reflect the proto-cluster population as a whole, which are more likely to be quiescent than field galaxies selected at the same stellar mass ($>3 \times 10^{10}\ M_\odot$). However, while the majority of proto-cluster members may be fading, they are not completely devoid of star-formation. Three of the proto-cluster mergers are detected in 24 μm with implied star-formation rates $>50\ M_\odot$ yr^{-1} (in the range of luminous infrared galaxies), and the minor companions are often blue in observed $J - H$. It is unclear if the currently star-forming proto-cluster galaxies will consume their gas reservoirs by $z \sim 1$, or if subsequent mergers with gas-rich galaxies can continue to fuel star-formation (Snyder et al. 2012; Rudnick et al. 2012). On the other hand, the two most massive proto-cluster mergers (19085, 18511) show no evidence for 24 μm emission or blue companions, and so may be truly "dry" mergers.

It is unlikely that the high merger rate observed in the center of XMM-LSS J02182-05102 could continue indefinitely. We suggest that the virialization of the proto-cluster may act as a mechanism to halt the assembly of the massive proto-cluster galaxies. The bulk of the assembly and star-formation of massive proto-cluster galaxies may occur before the virialization of host proto-cluster has completed. The massive galaxies will acquire enough mass such that subsequent mergers are likely to have higher mass ratios and therefore longer dynamical decay timescales. Galaxies in the local environment will become depleted unless they are replenished by the accretion of more groups onto the proto-cluster. The mass growth of the proto-cluster and its eventual virialization will in turn prevent the efficient accretion of satellites onto the more massive proto-cluster galaxies. The study of massive galaxies in a large sample of $z > 1.5$ overdensities with a range of masses and virialization states is needed to determine if accelerated galaxy assembly is a generic feature of proto-cluster systems.

We thank the referee and editor for their patience with this manuscript. We wish to acknowledge the members of the CANDELS, SEDS, and UKIDSS teams, and M. Cooper for their contributions to the data presented here. We thank E. Bell, D. Koo, B. Mobasher, J. Newman, L. Pentericci, A. Pope, B. Weiner, and S. Wuyts for helpful discussions and comments. This work is based on observations taken by the CANDELS Multi-Cycle Treasury Program with the NASA/ESA *HST*, which is operated by the Association of Universities for Research in Astronomy, Inc., under NASA contract NAS5-26555. This work is supported by *HST* program number GO-12060. Support for Program number GO-12060 was provided by NASA through a grant from the Space Telescope Science Institute, which is operated by the Association of Universities for Research in Astronomy, Incorporated, under NASA contract NAS5-26555. This work is based on observations made with the *Spitzer Space Telescope*, which is operated by the Jet Propulsion Laboratory, California Institute of Technology. This work is based in part on data obtained as part of the UKIRT Infrared Deep Sky Survey.

REFERENCES

Bassett, R., Papovich, C., Lotz, J. M., et al. 2013, ApJ, 770, 58
Bauer, A. E., Grützbauch, R., Jorgensen, I., Varela, J., & Bergmann, M. 2011, MNRAS, 411, 2009
Bell, E. F., Wolf, C., Meisenheimer, K., et al. 2004, ApJ, 608, 752
Bertin, E., & Arnouts, S. 1996, A&AS, 117, 393
Binney, J., & Tremaine, S. 1987, Galactic Dynamics (Princeton, NJ: Princeton Univ. Press), 428
Boylan-Kolchin, M., Ma, C.-P., & Quataert, E. 2005, MNRAS, 362, 184
Brammer, G., van Dokkum, P., & Coppi, P. 2008, ApJ, 686, 1503
Brammer, G., Whitaker, K. E., van Dokkum, P. G., et al. 2011, ApJ, 739, 24
Brough, S., Tran, K.-V., Sharp, R. G., von der Linden, A., & Couch, W. J. 2011, MNRAS, 414, 80
Brown, M. J. I., Dey, A., Jannuzi, B. T., et al. 2007, ApJ, 654, 858
Brown, M. J. I., Zheng, Z., White, M., et al. 2008, ApJ, 682, 937
Bruzual, G., & Charlot, S. 2003, MNRAS, 344, 1000
Bundy, K., Fukugita, M., Ellis, R. S., et al. 2009, ApJ, 697, 1369
Calzetti, D., Armus, L., Bohlin, R. C., et al. 2000, ApJ, 533, 682
Caputi, K., Dunlop, J. S., McLure, R. J., & Roche, N. D. 2005, MNRAS, 361, 607
Chabrier, G. 2003, PASP, 115, 763
Chary, R., & Elbaz, D. 2001, ApJ, 556, 562
Cimatti, A., Daddi, E., & Renzini, A. 2006, A&A, 453, 29
Civano, F., Elvis, M., Lanzuisi, G., et al. 2010, ApJ, 717, 209
Comerford, J., Pooley, D., Gerke, B. F., & Madejski, G. M. 2011, ApJL, 737, L19
Conroy, C., Wechsler, R., & Kravtsov, A. V. 2007, ApJ, 668, 826
Cooper, M. C., Griffith, R. L., Newman, J. A., et al. 2012, MNRAS, 419, 3018
de Lucia, G., & Blaziot, J. 2007, MNRAS, 375, 2
Faber, S. M., Willmer, C. N. A., Wolf, C., et al. 2007, ApJ, 665, 265
Fassbender, R., Nastasi, A., Böhringer, H., et al. 2011, A&A, 527, L10
Furusawa, H., Kosugi, G., Akiyama, M., et al. 2008, ApJS, 176, 1
Galametz, A., Grazian, A., Fontana, A., et al. 2013, ApJS, 206, 10
Gonzalez, A. H., Zaritsky, D., & Zabludoff, A. 2007, ApJ, 666, 147
Grogin, N. A., Kocevski, D. D., Faber, S. M., et al. 2011, ApJS, 197, 35
Hayashi, M., Kodama, T., Koyama, Y., et al. 2010, MNRAS, 402, 1980
Hudson, D. S., Reiprich, T. H., Clarke, T. E., & Sarazin, C. L. 2006, A&A, 453, 433
Ilbert, O., Salvato, M., Le Floc'h, E., et al. 2010, ApJ, 709, 644
Khochfar, S., & Burkert, A. 2003, ApJL, 597, L117
Kocevski, D., Lemaux, B. C., Lubin, L. M., et al. 2011, ApJ, 736, 38
Koekemoer, A. M., Faber, S. M., Ferguson, H. C., et al. 2011, ApJS, 197, 36
Komossa, S., Burwitz, V., Hasinger, G., et al. 2003, ApJL, 582, L15
Laidler, V., Papovich, C., Grogin, N. A., et al. 2007, PASP, 119, 1325
Lauer, T. 1988, ApJ, 325, 49
Lidman, C., Iacobuta, G., Bauer, A. E., et al. 2013, MNRAS, 433, 825
Lotz, J. M., Jonsson, P., Cox, T. J., & Primack, J. R. 2010, MNRAS, 404, 575
Lotz, J. M., Jonsson, P., Cox, T. J., et al. 2011, ApJ, 742, 103
Man, A. W. S., Toft, S., Zirm, A. W., Wuyts, S., & van der Wel, A. 2012, ApJ, 744, 85
Mancone, C., Gonzalez, A. H., Brodwin, M., et al. 2010, ApJ, 720, 298
Masjedi, M., Hogg, D. W., & Blanton, M. R. 2008, ApJ, 679, 260
McIntosh, D., Guo, Y., Hertzberg, J., et al. 2008, MNRAS, 338, 1537
Newman, A., Ellis, R. S., Bundy, K., & Treu, T. 2012, ApJ, 746, 162
Nipoti, C., Treu, T., Leauthaud, A., et al. 2012, MNRAS, 422, 1741
Oser, L., Naab, T., Ostriker, J. P., & Johansson, P. H. 2012, ApJ, 744, 63
Papovich, C. J. 2008, ApJ, 676, 206
Papovich, C. J., Bassett, R., Lotz, J. M., et al. 2012, ApJ, 750, 93
Papovich, C. J., Dickinson, M., & Ferguson, H. C. 2001, ApJ, 559, 620
Papovich, C. J., Momcheva, I., Willmer, C. N. A., et al. 2010, ApJ, 716, 1503
Papovich, C. J., Moustakas, L. A., Dickinson, M., et al. 2006, ApJ, 640, 92
Patton, D., & Atfield, J. E. 2008, ApJ, 685, 235
Pierre, M., Clerc, N., Maughan, B., et al. 2012, A&A, 540, 4
Rudnick, G., Tran, K.-V., Papovich, C., et al. 2012, ApJ, 755, 14
Rudnick, G., von der Linden, A., Pelló, R., et al. 2009, ApJ, 700, 1559
Rujopakarn, W., Rieke, G. H., Weiner, B. J., et al. 2013, ApJ, 767, 73
Scarlata, C., Carollo, C. M., Lilly, S. J., et al. 2007, ApJS, 172, 494
Simpson, C., Rawlings, S., Ivison, R., et al. 2012, MNRAS, 421, 3060
Smail, I., Sharp, R., Swinbank, A. M., et al. 2008, MNRAS, 389, 407
Smith, J. D. T., Draine, B. T., Dale, D. A., et al. 2007, ApJ, 656, 770
Snyder, G., Brodwin, M., Mancone, C. M., et al. 2012, ApJ, 756, 114
Snyder, G., Hayward, C. C., Sajina, A., et al. 2013, ApJ, 768, 168
Springel, V., White, S. D., Jenkins, A. D., et al. 2005, Natur, 435, 629
Stott, J. P., Collins, C. A., Sahlén, M., et al. 2010, ApJ, 718, 23
Tadaki, K., Kodama, T., Ota, K., et al. 2012, MNRAS, 423, 2617
Tanaka, M., Finoguenvo, A., & Ueda, Y. 2010, ApJL, 716, L156
Thomas, D., Maraston, C., Bender, R., & Mendes de Oliveira, C. 2005, ApJ, 621, 673
Tran, K.-V., Moustakas, J., Gonzalez, A. H., et al. 2008, ApJL, 683, L17
Tran, K.-V., Papovich, C., Saintonge, A., et al. 2010, ApJL, 719, L126
Tran, K.-V., van Dokkum, P., Franx, M., et al. 2005, ApJ, 627, 25
Van Dokkum, P., Pieter, G., Franx, M., et al. 1999, ApJ, 520, 95
White, M., Zheng, Z., Brown, M. J. I., Dey, A., & Jannuzi, B. T. 2007, ApJL, 655, L69
Williams, R. J., Quadri, R. F., & Franx, M. 2011, ApJL, 738, L25
Williams, R. J., Quadri, R. F., Franx, M., van Dokkum, P., & Labbé, I. 2009, ApJ, 691, 1879
Wuyts, S., Labbé, I., Franx, M., et al. 2007, ApJ, 655, 51
Zeimann, G. R., Stanford, S. A., Brodwin, M., et al. 2012, ApJ, 756, 115
Zirm, A., Toft, S., & Tanaka, M. 2012, ApJ, 744, 181